Author/s:
Kim, S;Heath, DE;Kentish, SE

Title:
Robust and Superhydrophobic PTFE Membranes with Crosshatched Nanofibers for Membrane Distillation and Carbon Dioxide Stripping

Date:
2022-08-01

Citation:
Kim, S., Heath, D. E. & Kentish, S. E. (2022). Robust and Superhydrophobic PTFE Membranes with Crosshatched Nanofibers for Membrane Distillation and Carbon Dioxide Stripping. Advanced Materials Interfaces, 9 (23), https://doi.org/10.1002/admi.202200786.

Persistent Link:
https://hdl.handle.net/11343/324529

ADVANCED MATERIALS INTERFACES
www.advmatinterfaces.de

Robust and Superhydrophobic PTFE Membranes with Crosshatched Nanofibers for Membrane Distillation and Carbon Dioxide Stripping

*Seungju Kim, Daniel E. Heath, and Sandra E. Kentish**

Polytetrafluoroethylene (PTFE) nanofiber membranes with novel crosshatched structures are developed and applied to both water desalination by direct contact membrane distillation (MD) and CO_2 separation by membrane gas absorption. Crosshatched structures are produced from a PTFE-poly(ethylene oxide)(PEO) emulsion by depositing alternating layers of aligned fibers oriented in perpendicular directions. This is followed by sintering to remove the PEO and to stabilize the structure. The crosshatched structure allows for rapid gas and vapor transport due to the low tortuosity and high porosity, leading to fast and effective separation. PTFE nanofiber membranes with these novel structures are ideal for membrane CO_2 stripping as this polymer is inherently strong and very hydrophobic. The mass transfer in both MD and CO_2 stripping is greatly improved in the crosshatched nanofibers (CNF) as well as in composite membranes with microparticles (CNF-MP), as compared with conventional random nanofibers. The membranes exhibit a MD flux up to 98.5 ± 1.2 kg $m^{-2}h^{-1}$, significantly greater than a standard PTFE membrane with asymmetric morphology, when tested with a 3.5 wt% sodium chloride feed solution at 80 °C in direct contact with water at 20 °C.

1. Introduction

Climate change has become a critical global issue, and a need for energy efficient and sustainable separation processes has arisen, to replace traditional energy-intensive industries. In this respect, membrane technology has emerged as an important approach to resource recovery, to deliver potable water through desalination and for carbon dioxide (CO_2) separation, which can provide solutions for carbon emissions from industrial sources.[1]

Electrospun nanofiber membranes have received increasing research focus in such applications as they offer remarkable flux due to their high porosity. As one example, these structures have been commercialized by Cytiva in their Fibro PrismA devices for pharmaceutical separations.[2] In electrospinning, electric forces draw polymer solutions into charged fibers that form a non-woven mat. Fiber properties such as layer thickness, fiber diameter, and porosity can be tailored.[3] Although standard electrospinning produces fibers in random orientation, the use of rotating collectors or parallel plate electrodes can fabricate the structures with highly aligned fibers for use in biomedical and reverse osmosis membrane applications.[4]

Membrane distillation (MD) is an emerging technology to thermally draw water vapor from a saline solution using a vapor pressure driving force at low temperatures of 50–80 °C. There is no limit to the salt concentrations in the feed in MD, so it can readily deal with hypersaline solutions for wastewater treatment and crystallizing solutions in the resource recovery industry.[3,5] A membrane is located between a hot feed and cold permeate to allow for vapor transport through the membrane pores. The membrane must be porous and hydrophobic to prevent membrane wetting, since liquid water condensed in membrane pores causes reduced flux rates, operational failure, and saline water permeation. Many workers have considered electrospun membranes in this application with considerable success.[3–6] For instance, polyvinylidene difluoride (PVDF) electrospun membranes have been investigated in MD due to their hydrophobic nature, mechanical strength, and facile processibility using common organic solvents.[5b] The use of 3D welding of the PVDF nanofibers can facilitate stable operation for 170 h using seawater as feed.[7] Other polymers such as polyimide have also been applied after surface modification to improve hydrophobicity.[8]

Membrane gas absorption (MGA) can be an ideal alternative for the currently dominant solvent absorption process for CO_2 capture due to its great mass transfer area per unit volume and low regeneration energy.[9] In this approach, a membrane separates the gas and solvent phases, providing for CO_2 transport during both absorption and stripping. Like MD, a hydrophobic membrane allows for permeation of CO_2 while rejecting transport of the solvent. MGA can even operate at low CO_2

S. Kim, S. E. Kentish
Department of Chemical Engineering
The University of Melbourne
Parkville, VIC 3010, Australia
E-mail: sandraek@unimelb.edu.au
D. E. Heath
Department of Biomedical Engineering
The University of Melbourne
Parkville, VIC 3010, Australia

The ORCID identification number(s) for the author(s) of this article can be found under https://doi.org/10.1002/admi.202200786.

DOI: 10.1002/admi.202200786

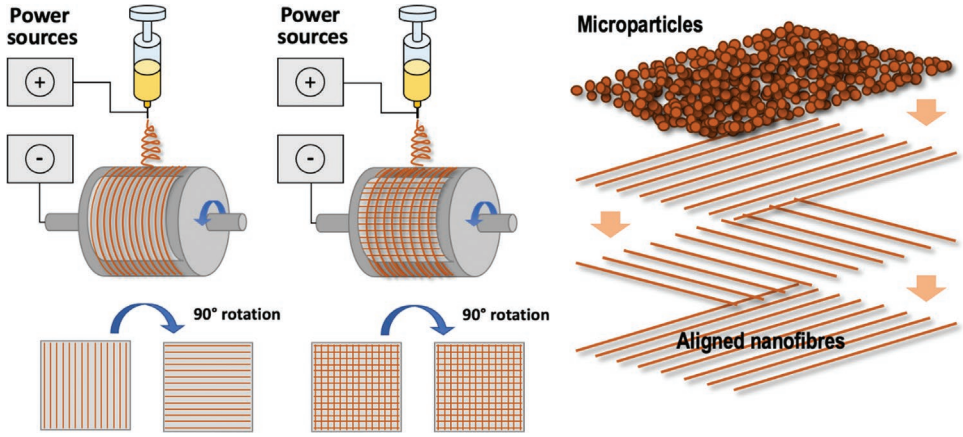

Figure 1. A schematic drawing of a crosshatched nanofiber membrane with microparticles to form composite structures.

concentrations and partial pressures, thus the technology is widely adaptable to a range of applications in CO_2 separation from biogas, syngas, natural gas, or flue gas from power generation.[10] Appropriate hydrophobicity is essential for the membranes since CO_2 transfer significantly decreases through wetted pores. PVDF nanofibers have also presented outstanding CO_2 stripping performance in MGA without wetting for 240 h.[10c]

Polytetrafluoroethylene (PTFE) is an attractive material for both these applications due to its great hydrophobicity and outstanding chemical stability.[6c,9] However, the insolubility of PTFE in conventional organic solvents has limited its use in membrane fabrication. Alternatively, PTFE nanofiber membranes prepared by emulsion electrospinning have been reported for MD,[6c,11] oil/water separation[12] and triboelectric generators.[13] A PTFE emulsion, containing poly(vinyl alcohol) (PVA) or poly(ethylene oxide) (PEO) to allow dissolution in a suitable solvent is used for electrospinning, then the pure PTFE nanofibers are obtained by high temperature sintering.

In this contribution, we demonstrate the fabrication of crosshatched structures of aligned nanofibers. These novel structures provide not only reduced tortuosity for fast molecular transport but improved mechanical strength in the direction of fiber orientation as compared to random nanofibers (RNF). PTFE nanofiber membranes are fabricated from a PTFE-PEO emulsion with subsequent sintering, then tested for both direct contact MD (DCMD) and CO_2 stripping within a gas absorption membrane contactor for MGA. We also fabricate PTFE composite nanofiber membranes with microparticles coated on the nanofiber mat to provide superhydrophobicity; by electrospraying prior to sintering.

2. Results and Discussion

2.1. Nanofiber Morphology and Physical Properties

Electrospinning is an electrically driven fabrication method for the production of fibers in micron to nanometer scales. As only high-quality continuous fibers of good mechanical strength can be applied in membrane applications, the electrospinning parameters such as electric field strength, solution conductivity, surface tension and viscosity, collector size, and shape, were first optimized to produce uniform nanofibers. Alternative parameters were also developed for the production of microparticles rather than fibers, which can be formed through electrospraying, where the fiber jet breaks up during flight, as the balance between viscoelastic forces, surface tension, and electrostatic repulsion is disrupted (**Figure 1**).[14] In emulsion electrospinning, solutions with low PEO concentrations (low viscosity) result in microparticles or bead-on-strings, evidenced by scanning electron microscope (SEM) images in Figure S1a–d, Supporting Information. Higher concentrations of PEO increase the solution viscosity and the solution forms uniform nanofibers (#5 to #7 in Table S1, Supporting Information). The low conductivity of the solution in the absence of LiCl as a conductivity booster (#8 and #9), results in solid polymers, rather than fibers. The applied voltage also affects the fiber morphology as high voltage produces nanofibers with small diameters and random orientation, as shown in Figure S2, Supporting Information. A low applied voltage improves the fiber alignment, but the nanofiber diameter becomes larger, of micron scale. For further electrospinning, the applied voltage for the needle tip and collector were fixed at +12 and −5 kV, respectively.

The rotating speed of the collector is a determining factor in nanofiber alignment and orientation (**Figure 2**). RNFs were formed from the solution #5 in Table S1, Supporting Information when the surface tangential speed was 80 cm s^{-1}, while partially aligned nanofibers were observed in the range of 300 and 1000 cm s^{-1}. On the other hand, well-aligned nanofibers were fabricated at a speed over 1400 cm s^{-1}. However, any further increase in tangential speed resulted in some airborne nanofibers in the electrospinning apparatus as the centrifugal forces on the collector exceeded the electric field forces. Therefore, the rotating speed was fixed at 1400 cm s^{-1} for the aligned nanofibers. The crosshatched nanofiber (CNF) membranes were obtained by forming layers of aligned nanofibers in two orthogonal directions and are referred to as CNFs. As a comparison, RNFs were prepared with a rotation speed at 80 cm s^{-1}. A layer of microparticles was electrosprayed on both RNF and CNF membranes to fabricate composite structures, referred to as CNF-MP and RNF-MP, respectively. This layer of microparticles is expected to improve hydrophobicity by increasing surface roughness and also provide a smaller pore size for liquid water at entry. The volume of the PTFE-PEO emulsion used for this

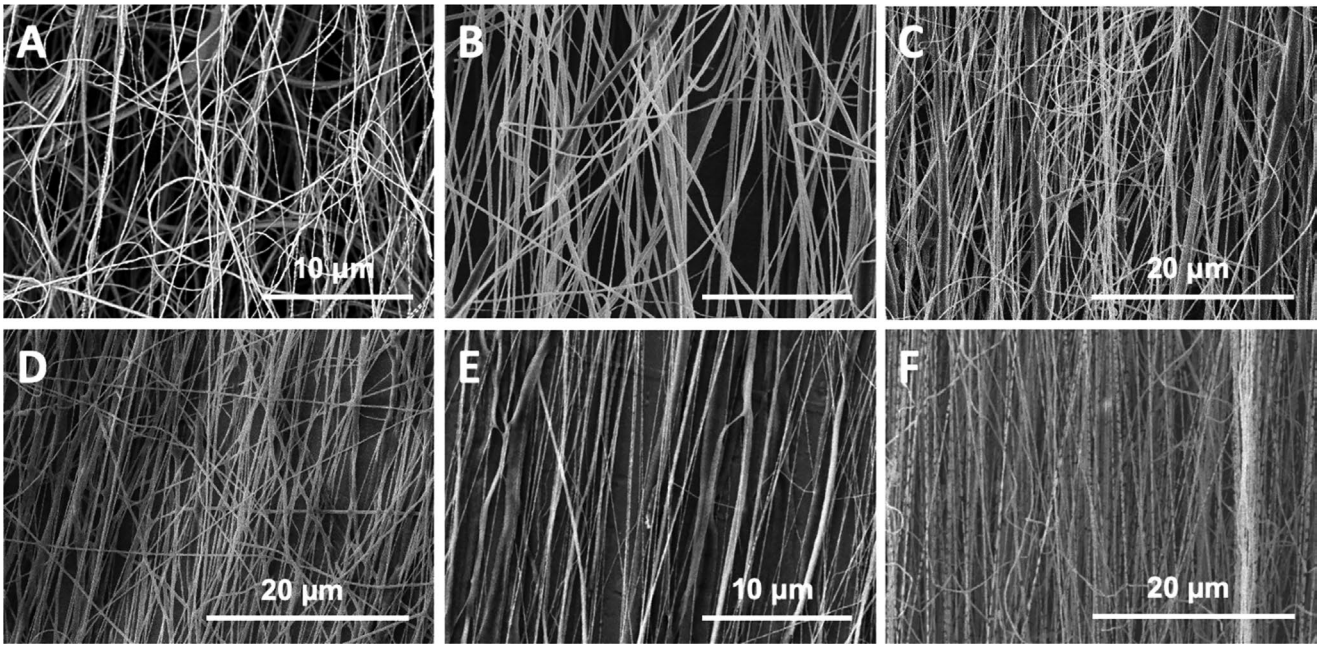

Figure 2. SEM images of PTFE-PEO electrospun membranes prepared at rotating speeds of A) 80, B) 300, C) 800, D) 1100, E) 1400, and F) 1600 cm s^{-1}.

step was determined by breakthrough pressure measurements. The breakthrough pressure gradually increased as more emulsion was applied, then reached an equilibrium once the microparticles completely covered the membrane surface.

The PTFE-PEO nanofiber membranes were then thermally treated to obtain PTFE nanofiber membranes. This thermal treatment also acted to enhance the adhesion between these microparticles and the underlying fibers. The treatment condition was confirmed by thermogravimetric analysis (TGA) (Figure S3, Supporting Information). Since PTFE has a much higher degradation temperature of 500 °C than PEO at 350 °C, the PEO in the PTFE-PEO blend can be easily eliminated. The decomposition of PEO was also confirmed by contact angle measurement (Figure S4, Supporting Information). Water droplets dissolved the PTFE-PEO nanofibers, but the PTFE nanofiber membranes showed a contact angle of around 144°, regardless of the nanofiber orientation. The color of the nanofibers also changed to light brown from white after sintering. SEM images confirmed that both CNF and RNF membranes have layers of aligned or random nanofibers with diameter of 300 nm (see **Figure 3**), while microparticles with diameter of 1.0 µm were uniformly deposited on the surface for CNF-MP and RNF-MP. The morphology and the size of the nanofibers and microparticles were unchanged after thermal treatment.

Water contact angle is an indicator for hydrophobicity, with a value over 150° regarded as superhydrophobic.[15] PTFE is known to show great hydrophobicity due to its fluorine-rich polymer chain, but the nanofibrous structures as well as the use of microparticles further improved the hydrophobicity, due to the existence of gas pockets between the nanofibers and the particles.[10c] The nanofiber membranes (RNF and CNF) exhibited a contact angle around 144° and the RNF-MP and CNF-MP showed around 153° (Figure S4B–E, Supporting Information), which is higher than that for a flat sheet commercial PTFE membrane at 140°. The nanofiber orientation, whether random or crosshatched, does not affect the surface hydrophobicity.

The number of layers of aligned nanofibers determines the membrane thickness, as shown in Figure S5, Supporting Information. However, the overall porosity is not influenced by the number of layers. The use of six layers provides a thickness of 62 µm, similar to that of the commercial asymmetric PTFE membrane (**Table 1**). Despite the similar thickness of all membranes, the nanofiber membranes have higher overall porosity (around 73%) than the asymmetric structure (33%). Nanofibrous structures are known to have very high porosity due to the space between nanofibers,[5b] and the microparticles on the surface do not affect the overall porosity due to this layer being very thin. However, the additional layer of tightly dispersed microparticles increases the breakthrough pressure of water and 2-propanol solution by reducing the maximum pore size of the composite membranes at liquid entry (d_{max}). The greater hydrophobicity induced by the microparticles also increases the water contact angle (Table 1) which further contributes to the greater breakthrough pressure. Again, due to the minimal thickness, the layer of microparticles does not affect the average pore size ($d_{average}$). The most distinguishing properties between the PTFE membranes are the tortuosity and structural parameters. Tortuosity is a measure of the shape of pores; a membrane with tortuosity of 1.0 has cylindrical straight pores which do not hinder molecular transport, while larger values suggest a longer pathway through the membrane structure.[4a] The high porosity and low tortuosity of the nanofiber membranes lead to a high pure water flux (Table 1; Equation S8, Supporting Information). The crosshatched morphology of the CNF membranes further decreased the membrane tortuosity in comparison to the RNF membranes. The structural parameter is defined from the Hagen–Poiseuille equation and describes the membrane resistance. Usually, membranes with a low S parameter exhibit less

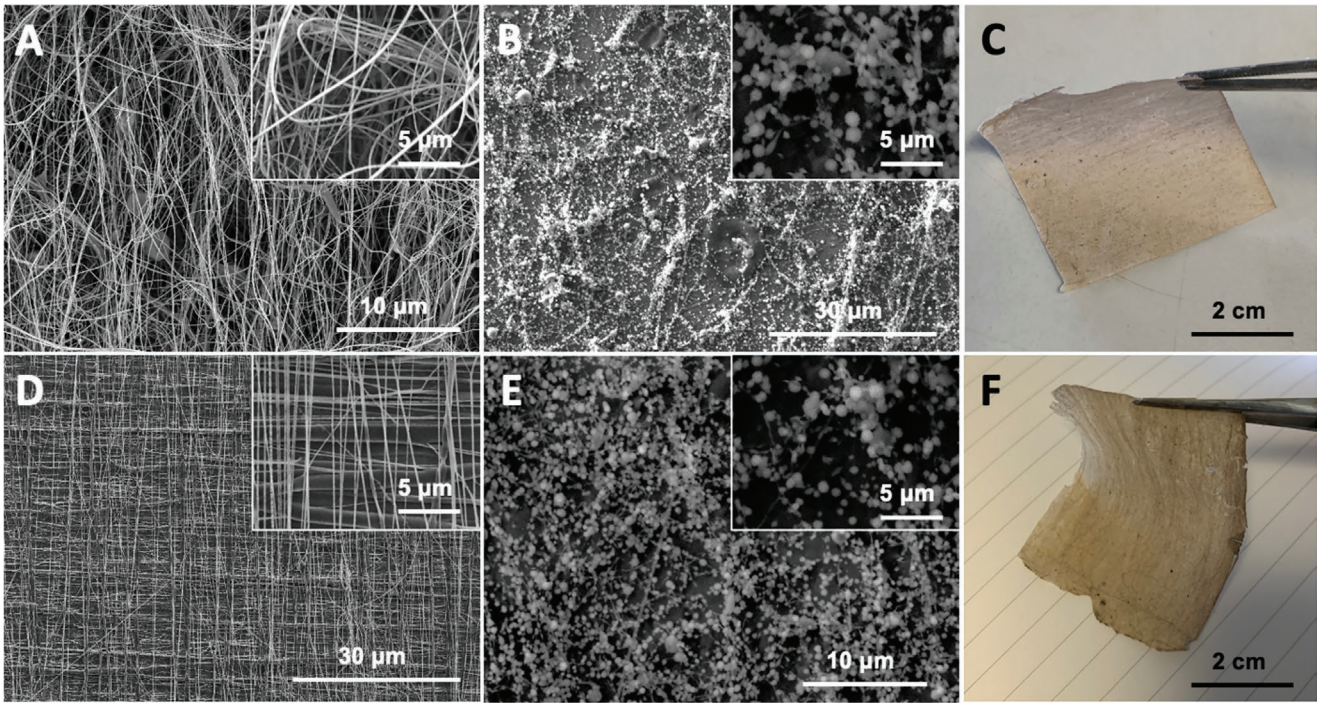

Figure 3. SEM and optical images of A) RNF, B) RNF-MP, C) RNF (optical), D) CNF, E) CNF-MP, and F) CNF (optical).

internal concentration polarization and stable flux in reverse osmosis and forward osmosis water treatment applications,[16] and this can also influence membrane performance in MD and MGA. The structural parameter of the commercial PTFE membrane was around ten times larger (1256 µm) than that of the nanofiber membranes at 102 to 148 µm, which would lead to slower molecular transport.

Electrospun nanofiber membranes usually have lower mechanical strength than asymmetric membranes which is one reason that they have been applied to processes such as MD and MGA, which use much lower feed pressures than traditional pressure-driven membrane processes.[3,5] A high mechanical strength of the membranes is, however, essential for ease of fabrication and to assist in increasing the membrane lifespan. We have recently shown that the novel crosshatched morphology used here greatly improved the mechanical strength of polysulfone (PSF) CNF used as a supporting layer for reverse osmosis membrane and operated at up to 50 bar.[4a] In the present case, RNF membranes showed good elasticity with an elongation at break of over 40%, but easily broke at low stress (**Figure 4**). These mechanical properties are similar to that of other PTFE nanofiber membranes reported in the literature as summarized in **Table 2**.[11,17] Conversely, the crosshatched orientation increased the tensile strength threefold, but

Table 1. The physical properties of the PTFE membranes.

	CNF	CNF-MP	RNF	RNF-MP	Asymmetric
Membrane thickness [µm]	62 ± 1	63 ± 1	63 ± 1	62 ± 1	64 ± 1
Overall porosity [%]	73 ± 1	72 ± 1	72 ± 1	73 ± 1	33 ± 2
Water contact angle [°]	144 ± 2	152 ± 1	144 ± 1	153 ± 2	140 ± 1
Water breakthrough pressure [kPa][a)]	115 ± 2	132 ± 4	119 ± 3	144 ± 2	220 ± 3
Contact angle of 2-propanol 50 wt% solution [°]	68 ± 2	69 ± 2	67 ± 3	69 ± 2	67 ± 2
Breakthrough pressure of 2-propanol solution [kPa]	38 ± 2	52 ± 2	40 ± 1	53 ± 1	110 ± 2
d_{max} by breakthrough pressure of 2-propanol solution [µm]	0.96	0.67	0.95	0.66	0.36
$d_{average}$ by N_2 permeance [µm]	0.63	0.59	0.54	0.52	0.23
Effective surface porosity [m^{-1}]	132	124	116	97	111
Pure water flux at 2 bar [L m^{-2} h^{-1} bar^{-1}][b)]	87 000 ± 1000	71 000 ± 300	46 000 ± 2000	41 000 ± 500	1180 ± 90
Tortuosity	1.20	1.26	1.62	1.74	6.48
Structural parameter [µm]	102	110	142	148	1256

[a)]Also known as critical entry pressure; [b)]At 2.5 bar for asymmetric.

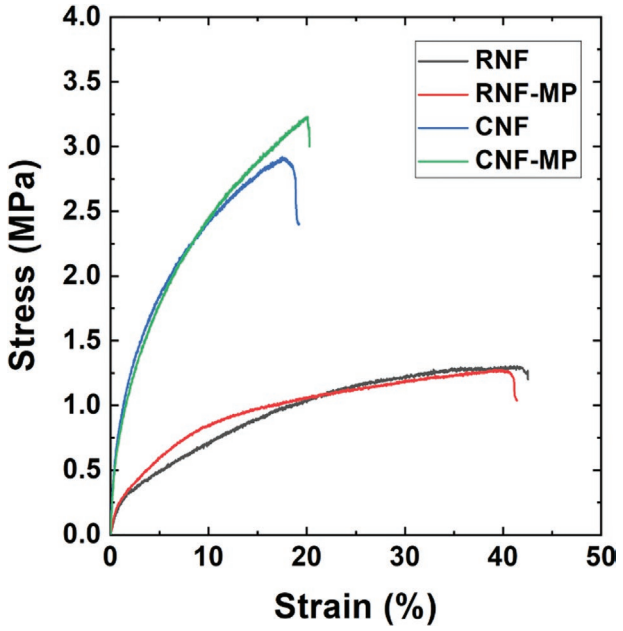

Figure 4. Typical mechanical properties of the nanofiber membranes. The average tensile strength and elongation at break of replicate samples is provided in Table 2.

with reduced elasticity since the aligned nanofibers restricted fiber stretching. Despite the reduced elasticity of CNF membranes, the increased tensile strength is highly advantageous for practical membrane separation applications as it ensures structural integrity during module fabrication and provides resilience against abrasion from coarse contaminants such as sand.

2.2. Membrane Distillation

The effectiveness of these membranes for MD was investigated using a 3.5 wt% sodium chloride (NaCl) solution, indicative of seawater, as a feed and deionized (DI) water as a permeate in a DCMD setup. The measurement was conducted at feed temperatures of 50 to 80 °C with the permeate temperature fixed at 20 °C. For all the membranes studied here, the MD water flux increased as a function of feed temperature due to the increased vapor pressure (**Figure 5**A). When the ΔT was 60 °C, the water flux of the CNF-MP membrane reached 98.5 ± 1.2 kg m^{-2} h^{-1}, which is 170% higher than that of the commercial asymmetric membrane at 58.2 ± 0.6 kg m^{-2} h^{-1}. Increasing the feed temperature further is not practical due to the intensive energy usage and possible membrane wetting. For all temperature differences, the water flux increased in the order of CNF-MP, CNF, RNF-MP and asymmetric. As shown by the Carman–Kozeny equation (Equation S10, Supporting Information), permeability increases with porosity and is inversely proportional to the square of the tortuosity.[18] The higher water flux of the nanofiber membranes relative to the asymmetric structure is due to the higher overall porosity as well as reduced tortuosity (Table 1). Similarly, it is the reduced tortuosity in the crosshatched structures that increases water flux, relative to the random arrangement. As reported previously, membranes with larger pore sizes tend to experience membrane wetting more frequently due to the water molecules easily penetrating the pores.[19] However, the nanofibrous structures with higher porosity and strong hydrophobicity here result in increased water flux. The improved water flux with the layer of microparticles on both RNF and CNF is attributed to the high effective evaporation area (EEA). As discussed by Park et al.,[20] a large EEA can be obtained with high water contact angles and small surface pore sizes, as is the case when this layer is applied. Further, a high contact angle can reduce the likelihood of crystallization on the membrane surface.[20]

Table 2. Mechanical properties of the PTFE nanofiber membranes.

	Tensile strength [MPa]	Elongation at break [%]	Reference
PTFE RNF	1.3 ± 0.1	42 ± 2	This study
PTFE RNF-MP	1.3 ± 0.2	41 ± 3	This study
PTFE CNF	3.1 ± 0.2	18 ± 1	This study
PTFE CNF-MP	3.2 ± 0.2	20 ± 2	This study
PTFE	1.6	20	[17a]
PTFE-POSS	2.6	13	[17a]
PTFE	1.4	15	[11]
PTFE	1.0	47	[17b]

The water flux and salt rejection of the membranes were compared with other hydrophobic nanofiber membranes at the same operation conditions when the ΔT is 40 °C (20 °C for permeate and 60 °C for feed of 3.5 wt% NaCl solution). Although all membranes exhibited similarly high salt rejection (over 99.95%), the water flux of the PTFE membranes in this study was much higher than other hydrophobic nanofiber membranes and their nanocomposite or polymer blends. The high thermal conductivity of PTFE (around 0.4 W m K^{-1}) might be expected to cause more temperature polarization in the membrane, leading to reduced water flux[6a] but the high porosity and hydrophobicity of PTFE is clearly dominant here. PVDF-based nanofibers are frequently reported due to their ease in solution preparation, but PVDF is inherently less hydrophobic than PTFE, so that the water flux is lower.

Nanocomposite membranes with hydrophobic particles such as silica or polyhedral oligomeric silsesquioxanes (POSS) are often reported with similarly improved water flux,[17a] but the long-term structural stability can be an issue due to delamination or particle detachment. The nanofiber structures studied here exhibit much improved water flux without the need for additional hydrophobic microparticles or post surface treatment.

The water flux of the PTFE nanofiber membranes was also investigated with different feed solution of up to 300 g L^{-1} NaCl as described in **Figure 6**. All membranes demonstrated stable water flux for up to 7 wt% NaCl, but a flux decline was observed when this concentration increased to 15 and 23 wt% (175 and 300 g L^{-1}). This decline is partly related to the reduced water vapor pressure above concentrated salt solutions,[5a] which reduces the driving force.[22] The greater decline at 23 wt% also suggests crystallization of NaCl is occurring on

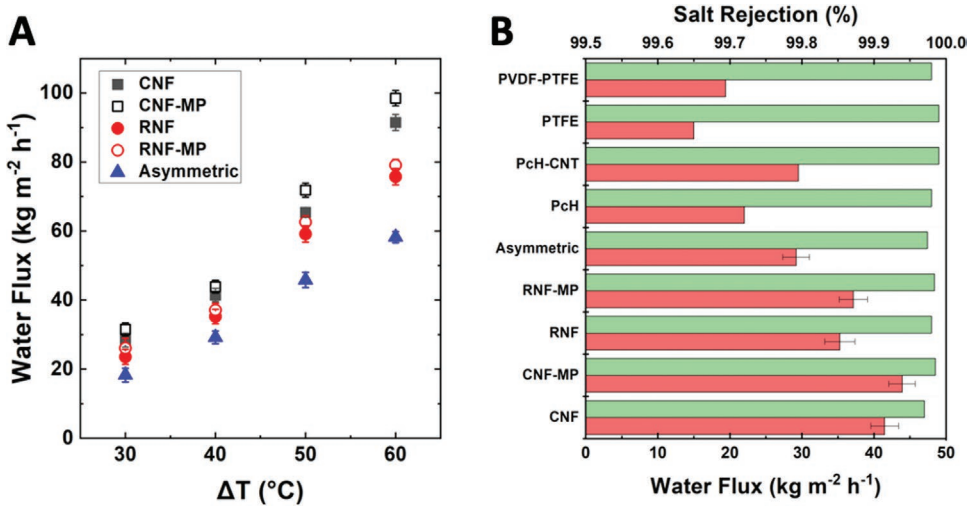

Figure 5. Water flux and salt rejection of PTFE nanofiber membranes with 3.5 wt% NaCl solution as feed, A) as a function of the temperature difference and B) as a comparison to other hydrophobic nanofiber membranes when the ΔT is 40 °C (PVDF-co-hexafluoropropylene (PcH) with carbon nanotubes (CNT),[15] PTFE,[17a] and PVDF-PTFE blend[21]), where the green bars are the rejection values and the red bars are the flux. Error bars represent ± one standard deviation, based on three replicate membranes.

the membrane surface, as the solubility limit is reached. These crystals block the pores, resulting in water flux decline. In some cases, such crystallization is desirable, such as in the pharmaceutical industry or for mineral recovery from hypersaline feeds.[5] If undesirable, such as for potable water production, pore blockage can be reduced by increasing the circulation velocity. Across the range of experimental conditions, all membranes maintained the initial salt rejection around 99.97% and no visual crystals were observed on the membrane surface. The water flux decline at high feed concentrations was less severe with the nanofiber membranes due to the higher porosity. The layer of microparticles might be expected to cause greater pore blockage by crystals, but no significant difference in the flux decline was detected at the higher feed concentrations.

Long-term performance stability can be the most critical property for MD membranes to be applied for practical operations. Many membranes fail due to the water flux decline by pore wetting that allows the permeation of salt over time.[23] **Figure 7** presents the water flux and NaCl rejection of CNF-MP, RNF-MP, and asymmetric PTFE membrane during continuous operations up to 200 h at 20 °C for permeate and 60 °C

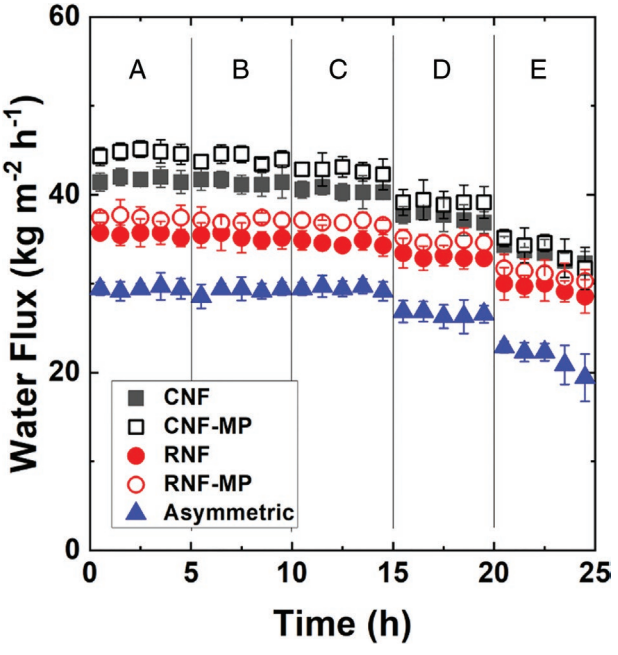

Figure 6. Water flux in DCMD operations with the use of different feed solutions of A) purified water, NaCl solution of B) 3.5, C) 7.0, D) 15 (175 g L^{-1}), and E) 23 wt% (300 g L^{-1}). Error bars represent ± one standard deviation, based on three replicate membranes.

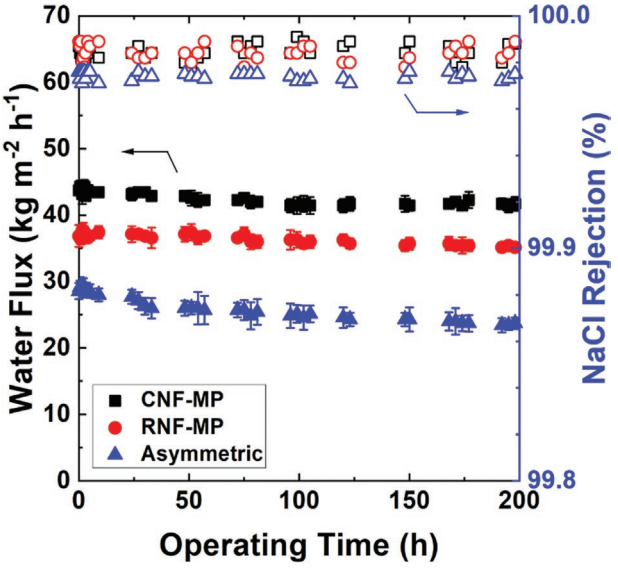

Figure 7. MD performance of PTFE membranes over an extended operation time with 3.5 wt% NaCl solution as feed. Error bars represent ± one standard deviation, based on three replicate membranes.

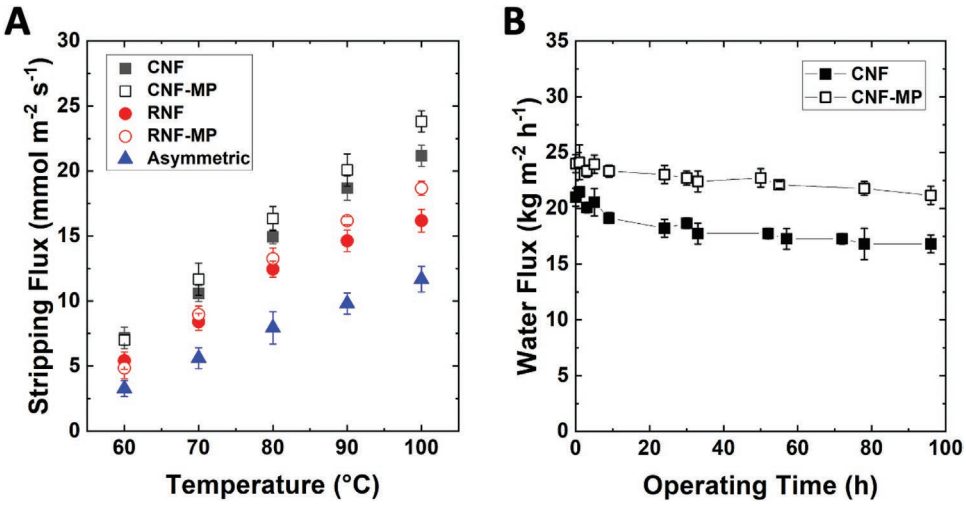

Figure 8. CO_2 stripping flux of PTFE membranes A) as a function of applied temperature and B) long-term performance measured at 100 °C with a solvent flowrate of 100 mL min^{-1} and gas flowrate of 70 mL min^{-1}. Error bars represent ± one standard deviation, based on three replicate membranes.

for feed of 3.5 wt% NaCl solution. Over the testing period, both CNF-MP and RNF-MP membranes demonstrated almost unchanged water flux (around 4% decline, within the error range of the experiments) and salt rejection. Microparticles can be detached from the nanofibers over time due to poor adhesion.[10c] However in the current PTFE composite membranes, the use of a sticky PEO solution and the subsequent thermal treatment led to strong adhesion, maintaining the composite structure during operation. The flux decline for the PTFE asymmetric membrane was similarly around 4% with the low porosity and small pore sizes preventing membrane wetting.

2.3. CO_2 Stripping

MGA for carbon capture consists of two membrane-based processes; absorption to remove CO_2 from the feed at around 30 °C and stripping to release the pure CO_2 from the absorbent at around 100 °C for sequestration. The CO_2 stripping process is more energy-intensive and challenging as a membrane application, as membrane wetting can readily occur due to the increased vapor pressure of the aqueous solution at high temperature, which can result in water re-condensing in the pores. The membrane properties required for MGA are identical to that for the MD process to reduce these wetting effects.[9] The PTFE nanofiber membranes were thus also applied to CO_2 stripping using a potassium glycinate (PG) solution as the absorbent. PG is an amino acid salt with a high reaction rate for CO_2 absorption that is regarded as an attractive absorbent to replace monoethanolamine (MEA) or diethanolamine (DEA) due to its lower environmental impact and resistance to degradation by oxidation.[24] Moreover, the low volatility of PG reduces absorbent loss during the membrane stripping step.[25] CO_2 absorption into PG is known to be via an exothermic zwitterionic reaction mechanism to produce a carbamate. At higher temperatures, this carbamate can thermally release CO_2 and return to an amine form.[24]

When the membranes were tested between 60 and 100 °C, the stripping flux increased as a function of temperature (**Figure 8**A), which is a similar trend to the MD process in Figure 5A. The PTFE nanofiber membranes exhibited a higher stripping flux than the asymmetric membranes due to their high porosity and pore sizes. In particular, the CNF membranes with crosshatched structures showed even higher flux than RNF membranes based on the less tortuous pore structures. Similar to MD, the microparticles coated on the nanofibers improved the surface hydrophobicity, leading to higher CO_2 stripping flux.

Long-term CO_2 stripping performance was also measured for the CNF membranes for 100 h as described in Figure 8B. The CNF membrane experienced a flux decline around 10% within 10 h, probably due to partial membrane wetting, similar to most membranes designed for MGA. However, the CNF-MP membranes demonstrated more constant flux for up to 100 h. The additional layer of microparticles improved hydrophobicity and reduced the liquid entry pore size sufficiently to prevent the solvent entering the membrane pores. Moreover, the microparticles were firmly attached on the nanofibers by thermal curing, so that the composite structure was stable during operation.

The CO_2 stripping performance of the PTFE nanofiber membranes generally exceeds that of membranes reported in the literature as summarized in **Table 3**.[10c,26] Most membranes reported are polymeric hollow fiber membranes with asymmetric structures, so that the stripping flux is usually lower than nanofiber membranes. Polymers with high solubility in organic solvents, such as PVDF, polyetherimide (PEI), or PSF are often studied due to the ease in fabrication, but the PTFE membranes with higher hydrophobicity usually present better performance in CO_2 stripping.

3. Conclusion

Crosshatched and composite structures of PTFE nanofibers were successfully fabricated using emulsion electrospinning,

Table 3. CO_2 stripping properties of the membranes in MGA.

Membrane	Type	Solvent	Temperature [°C]	CO_2 Flux [mmol m^{-2} s^{-1}]	Reference
PTFE CNF-MP	Nanofiber	30 wt% PG	80	16 ± 0.9	This study
			100	24 ± 0.8	This study
PTFE CNF	Nanofiber	30 wt% PG	80	15 ± 0.5	This study
			100	21 ± 0.8	This study
PTFE RNF-MP	Nanofiber	30 wt% PG	80	19 ± 0.5	This study
PTFE RNF	Nanofiber	30 wt% PG	80	16 ± 0.9	This study
PTFE	Hollow fiber	5 M MEA	100	1.3	[26b]
PTFE	Flat sheet	30 wt% K_2CO_3	100	13	[26c]
PVDF-HFP	Nanofiber	30 wt% PG	80	9.8	[10c]
PVDF-HFP-BS	Nanofiber	30 wt% PG	80	11	[10c]
PVDF-HFP	Hollow fiber	10 wt% DEA	80	8	[26a]
PEI	Hollow fiber	1 M DEA	80	13	[26d]
PSF	Hollow fiber	1 M MEA	80	0.12	[26e]
PDMS on PSF	Hollow fiber	30 wt% MEA	100	1	[26f]
Al_2O_3	Hollow fiber	5 M MEA	80	2.56	[26g]
α-Al_2O_3	Tubular	5 M MEA	100	1.17	[26h]

resulting in membranes of low tortuosity and superhydrophobicity. The use of a rotating drum collector during electrospinning produced nanofibers with well-aligned orientation, with the crosshatched layers then obtained by alternating layers of perpendicularly aligned nanofibers. The PTFE nanofiber membranes demonstrated remarkable water flux and salt rejection in DCMD operations at 50 to 80 °C using NaCl solution of up to 300 g L^{-1}; and for over 200 h of continuous operation. These membranes also demonstrated improved CO_2 stripping flux in MGA operations using an amino acid CO_2 absorbent. The reduced resistance to gas and vapor flow of the CNF layer effectively improved these fluxes when compared to RNFs of similar porosity and thickness. Composite structures of microparticles adhered to the nanofiber layers also increased water breakthrough pressure as well as surface hydrophobicity which critically improved long-term performance stability; without detachment of the microparticles over time. The fabrication methods for the PTFE nanofiber and composite membranes are readily scaled to larger manufacturing processes using existing electrospinning technology. Constant rotation of around 1400 cm s^{-1} is required for aligned nanofibers, but this speed is achievable with large size drums. Other alignment techniques can also be applied such as the use of conductive wires or plates,[27] meaning that the membranes can readily be applied to practical applications for water desalination and CO_2 capture.

4. Experimental Section

Preparation of Hydrophobic Nanofiber Membranes: PTFE-PEO nanofibers were electrospun from an aqueous emulsion. The emulsion was prepared by dissolving PEO into an aqueous emulsion of 60 wt% PTFE at room temperature under vigorous stirring. Solid LiCl was also added as a conductivity booster. Details of the compositions used are listed in Table S1, Supporting Information. Once the solid PEO was completely dissolved, bubbles in the emulsion were removed by holding at room temperature overnight. The polymer emulsions were electrospun in a lab-scale electrospinning apparatus, consisting of a syringe pump with a single spray needle (Adelab Scientific, Thebarton, Australia), a rotating steel drum collector with diameter of 15 cm and length of 15 cm, and two high voltage power supplies (Spellman CZE1000R, Hauppauge, NY) for positive and negative voltage. The syringe pump was moved on the rail of a Linear Translation Stage (Thorlabs Inc., Newton, NJ) at 10 cm min^{-1}. The distance between the needle tip and collector was 10 cm. The needle was charged at +12 and −5 kV at the drum collector. The collector was rotated at a surface tangential speed of 80 to 1600 cm s^{-1} (200 to 2000 rpm) to investigate the effect on nanofiber orientation. From these studies, emulsion #5 (Table S1, Supporting Information) and a rotation speed of 1400 cm s^{-1} was selected for aligned nanofibers. A square coupon of aluminium foil (15 × 15 cm^2) was attached to the collector and 0.7 mL of the solution was injected at 1.0 mL h^{-1} to form a layer of aligned nanofibers upon this foil. It was then detached, replaced at 90° to the original position; and the same amount of solution was electrospun for the next layer of nanofibers. The procedure was repeated for the six layers of the aligned nanofibers to give membrane thickness of around 62 µm, similar to the commercial PTFE membrane. As a comparison, nanofiber membranes in random orientation were prepared through injection of 4.2 mL of solution at a rotation speed of 80 cm s^{-1}. Microparticles were electrosprayed on both nanofiber membranes from a lower viscosity emulsion (#1 in Table S1, Supporting Information). In this case, 0.5 mL of the emulsion was deposited to cover the entire surface of the nanofibers with minimal change to the overall membrane thickness.

The prepared membranes were thermally treated at 410 °C for 10 min at a heating rate of 3 °C min^{-1} under an argon atmosphere using a tubular furnace (STF1200 Tube Furnace, Across International, Livingston, NJ), to allow the PEO to decompose. The resulting pure PTFE nanofiber membranes were rinsed with purified water to remove residual LiCl and decomposed PEO before further characterization.

Characterization: The thermal treatment conditions for PEO decomposition were confirmed by TGA using a TG 209 F1 Libra, (NETZSCH-Gerätebau GmbH, Selb, Germany) under a nitrogen atmosphere at 5 °C min^{-1}. SEM (FlexSEM, Hitachi, Tokyo, Japan) was used to investigate the membrane morphology. The membrane

hydrophobicity was characterized from the water contact angle with a tensiometer (OCA 20, DataPhysics Instruments, Filderstadt, Germany). The mechanical strength in elongation and the tensile strength was measured using a universal testing machine (Model 5944 2 kN, Instron, Norwood, MA) with three replicate specimens according to the ASTM D638 standard. The breakthrough pressure (p_B) was measured with a dead-end filtration cell (HP4750, Sterlitech, Kent, WA), that was modified to visualize water droplets at the permeate surface.

Water Desalination by DCMD: Water flux and salt rejection in DCMD was measured using a lab-scale test unit as described in Figure S6, Supporting Information. The crossflow PTFE membrane holder with effective membrane area of 42 cm^2 (CF042P, Sterlitech, Auburn, WA) was assembled for counter-current flow of the feed and permeate stream (Micropump 83589 GC-M35.PVS5, Micropump Inc., Vancouver, WA). The permeate temperature was maintained at 20 °C and the feed temperature was controlled between 50 and 80 °C. The permeate solutions was purified water, while aqueous solutions of NaCl at 3.5, 7.0, 15, and 23 wt% were used as feed solutions. The flowrate at the feed and permeate was 10 mL min^{-1} at a countercurrent flow. The NaCl concentration of both the feed and permeate solutions was determined by a conductivity meter (SevenExcellence, Mettler Toledo, Columbus, OH). Purified water was added to the feed solution as permeation continued, to ensure a constant concentration, as indicated by this conductivity.

CO_2 Stripping by MGA: A flat sheet membrane arrangement was employed to investigate CO_2 stripping performance, as described in Figure S7, Supporting Information.[28] The stainless-steel membrane holder had an effective membrane area of 14.6 cm^2 and was manufactured in-house with channels for gas and solvent flow in a counter-current direction. The upper chamber contained a magnetically driven mechanical stirrer (Heidolph Instruments, Model RZR 2020, Germany) operating at 100 rpm to generate turbulence in the liquid phase. The temperature of the holder and gas flow channels was controlled in a range of 60 and 100 °C by placement in a convection oven. 30 wt% PG solution was prepared as a CO_2 absorbent from glycine and potassium hydroxide in equimolar quantities dissolved in purified water. The initial pH of the solution was 14 but this was lowered to pH 10 by bubbling CO_2 gas through the solution. This CO_2 loaded solution was injected into the solvent chamber at 100 mL min^{-1} using a peristaltic pump (MasterFlex L/S, Cole-Parmer, Vernon Hills, IL). N_2 gas at 70 mL min^{-1} was employed as a sweep at the gas chamber. The stripping flux was measured using the solvent flowrate and the solvent CO_2 concentration at the inlet and outlet stream, determined by titration with H_2SO_4 solution and methyl orange indicator.[10c]

Statistical Analysis: All measurements including mechanical properties, water desalination and CO_2 stripping were conducted with three replicate specimens. All data are expressed as the mean ± one standard deviation with a p-value < 0.05. OriginPro 2019b (OriginLab, Northampton, MA) and Microsoft Excel 16.61 (Microsoft, Redmond, WA) were used for statistical analysis.

Supporting Information

Supporting Information is available from the Wiley Online Library or from the author.

Acknowledgements

This research was supported under the Australian Research Council Discovery Projects Scheme (Project number DP190102253). The authors acknowledge the staff of the Materials Characterization and Fabrication Platform (MCFP) at the University of Melbourne and the Victorian Node of the Australian National Fabrication Facility (ANFF) for their technical assistance.

Open access publishing facilitated by The University of Melbourne, as part of the Wiley - The University of Melbourne agreement via the Council of Australian University Librarians.

Conflict of Interest

The authors declare no conflict of interest.

Data Availability Statement

The data that support the findings of this study are available from the corresponding author upon reasonable request.

Keywords

CO_2 stripping, electrospinning, membrane contactor, membrane distillation

Received: April 11, 2022
Revised: May 19, 2022
Published online: July 17, 2022

[1] a) H. Lu, W. Shi, F. Zhao, W. Zhang, P. Zhang, C. Zhao, G. Yu, *Adv. Funct. Mater.* **2021**, *31*, 2101036; b) M. Sun, C. Boo, W. Shi, J. Rolf, E. Shaulsky, W. Cheng, D. L. Plata, J. Qu, M. Elimelech, *Adv. Funct. Mater.* **2019**, *29*, 1903125; c) S. Kim, R. Ou, Y. Hu, X. Li, H. Zhang, G. P. Simon, H. Wang, *J. Membr. Sci.* **2018**, *562*, 47; d) S. Kim, S. H. Han, Y. M. Lee, *J. Membr. Sci.* **2012**, *403*, 169; e) S. Kim, H. Wang, Y. M. Lee, *Angew. Chem., Int. Ed.* **2019**, *131*, 17674; f) S. Kim, X. Lin, R. Ou, H. Liu, X. Zhang, G. P. Simon, C. D. Easton, H. Wang, *J. Mater. Chem. A* **2017**, *5*, 1533; g) R. Ou, H. Zhang, S. Kim, G. P. Simon, H. Hou, H. Wang, *Ind. Eng. Chem. Res.* **2017**, *56*, 505.

[2] Cytiva, Overcome Chromatography Challenges with Fiber Adsorbents, https://www.cytivalifesciences.com/en/us/solutions/bioprocessing/knowledge-center/chromatography-productivity-with-fiber-adsorbents (accessed: May 2022).

[3] L. D. Tijing, J.-S. Choi, S. Lee, S.-H. Kim, H. K. Shon, *J. Membr. Sci.* **2014**, *453*, 435.

[4] a) S. Kim, D. E. Heath, S. E. Kentish, *ACS Appl. Mater. Interfaces* **2020**, *12*, 44720; b) H. Han, H. Hong, S. M. Park, D. S. Kim, *Adv. Mater. Interfaces* **2020**, *7*, 2000571; c) K.-K. Yan, L. Jiao, S. Lin, X. Ji, Y. Lu, L. Zhang, *Desalination* **2018**, *437*, 26.

[5] a) K. L. Hickenbottom, T. Y. Cath, *J. Membr. Sci.* **2014**, *454*, 426; b) J. H. Kim, S. H. Park, M. J. Lee, S. M. Lee, W. H. Lee, K. H. Lee, N. R. Kang, H. J. Jo, J. F. Kim, E. Drioli, *Energy Environ. Sci.* **2016**, *9*, 878.

[6] a) S. Al-Obaidani, E. Curcio, F. Macedonio, G. Di Profio, H. Al-Hinai, E. Drioli, *J. Membr. Sci.* **2008**, *323*, 85; b) T.-D. Lu, B.-Z. Chen, J. Wang, T.-Z. Jia, X.-L. Cao, Y. Wang, W. Xing, C. H. Lau, S.-P. Sun, *J. Mater. Chem. A* **2018**, *6*, 15047; c) M. Xu, J. Cheng, X. Du, Q. Guo, Y. Huang, Q. Huang, *J. Membr. Sci.* **2022**, *641*, 119876; d) Z.-Q. Dong, X.-h. Ma, Z.-L. Xu, W.-T. You, F.-b. Li, *Desalination* **2014**, *347*, 175; e) M. Essalhi, M. Khayet, *J. Membr. Sci.* **2013**, *433*, 167; f) L. Eykens, K. De Sitter, C. Dotremont, L. Pinoy, B. Van der Bruggen, *Desalination* **2016**, *392*, 63; g) Q.-L. Huang, Y. Huang, C.-F. Xiao, Y.-W. You, C.-X. Zhang, *J. Membr. Sci.* **2017**, *534*, 73.

[7] L. Zhong, L. An, Y. Han, Z. Zhu, D. Liu, D. Liu, D. Zuo, W. Wang, J. Ma, *Environ. Sci. Technol.* **2021**, *55*, 11308.

[8] Z. Zhu, Y. Liu, H. Hou, W. Shi, F. Qu, F. Cui, W. Wang, *Environ. Sci. Technol.* **2018**, *52*, 3027.

[9] S. Kim, C. A. Scholes, D. E. Heath, S. E. Kentish, *Chem. Eng. J.* **2021**, *411*, 128468.

[10] a) C. A. Scholes, S. E. Kentish, G. W. Stevens, D. deMontigny, *Int. J. Greenhouse Gas Control* **2015**, *42*, 66; b) E. Hosseini, E. Soroodan Miandoab, G. W. Stevens, C. A. Scholes, *Sep. Purif. Technol.* **2020**,

249, 117151; c) S. Kim, D. E. Heath, S. E. Kentish, *Chem. Eng. J.* **2022**, *428*, 131247; d) S. Kim, D. E. Heath, W. H. Lee, Y. M. Lee, S. E. Kentish, *J. Membr. Sci.* **2022**, *654*, 120518.

[11] T. Zhou, Y. Yao, R. Xiang, Y. Wu, *J. Membr. Sci.* **2014**, *453*, 402.

[12] W. Qing, X. Shi, Y. Deng, W. Zhang, J. Wang, C. Y. Tang, *J. Membr. Sci.* **2017**, *540*, 354.

[13] P. Zhao, N. Soin, K. Prashanthi, J. Chen, S. Dong, E. Zhou, Z. Zhu, A. A. Narasimulu, C. D. Montemagno, L. Yu, J. Luo, *ACS Appl. Mater. Interfaces* **2018**, *10*, 5880.

[14] a) Z. Wang, C. Zhao, Z. Pan, *J. Colloid Interface Sci.* **2015**, *441*, 121; b) M. M. Munir, A. B. Suryamas, F. Iskandar, K. Okuyama, *Polymer* **2009**, *50*, 4935.

[15] L. D. Tijing, Y. C. Woo, W.-G. Shim, T. He, J.-S. Choi, S.-H. Kim, H. K. Shon, *J. Membr. Sci.* **2016**, *502*, 158.

[16] P. Xiao, L. D. Nghiem, Y. Yin, X.-M. Li, M. Zhang, G. Chen, J. Song, T. He, *J. Membr. Sci.* **2015**, *481*, 106.

[17] a) J. Ju, K. Fejjari, Y. Cheng, M. Liu, Z. Li, W. Kang, Y. Liao, *Desalination* **2020**, *486*, 114481; b) Y. Liang, J. Ju, N. Deng, X. Zhou, J. Yan, W. Kang, B. Cheng, *Appl. Surf. Sci.* **2018**, *442*, 54.

[18] a) A. Koponen, M. Kataja, J. Timonen, *Phys. Rev. E: Stat., Nonlinear, Soft Matter Phys.* **1997**, *56*, 3319; b) K. M. Graczyk, M. Matyka, *Sci. Rep.* **2020**, *10*, 21488.

[19] a) M. M. A. Shirazi, A. Kargari, M. Tabatabaei, *Chem. Eng. Process.: Process Intensif.* **2014**, *76*, 16; b) S. Adnan, M. Hoang, H. Wang, Z. Xie, *Desalination* **2012**, *284*, 297; c) D. Hou, J. Wang, D. Qu, Z. Luan, X. Ren, *Sep. Purif. Technol.* **2009**, *69*, 78.

[20] S. H. Park, J. H. Kim, S. J. Moon, E. Drioli, Y. M. Lee, *J. Membr. Sci.* **2018**, *550*, 545.

[21] J. Li, L. F. Ren, J. Shao, M. Adeel, Y. Tu, Z. Ma, Y. He, *J. Appl. Polym. Sci.* **2020**, *137*, 48467.

[22] R. W. Schofield, A. G. Fane, C. J. D. Fell, R. Macoun, *Desalination* **1990**, *77*, 279.

[23] H. Chamani, J. Woloszyn, T. Matsuura, D. Rana, C. Q. Lan, *Prog. Mater. Sci.* **2021**, *122*, 100843.

[24] D. Guo, H. Thee, C. Y. Tan, J. Chen, W. Fei, S. Kentish, G. W. Stevens, G. da Silva, *Energy Fuels* **2013**, *27*, 3898.

[25] V. S. Sefidi, P. Luis, *Ind. Eng. Chem. Res.* **2019**, *58*, 20181.

[26] a) S. Hosseini, A. Mansourizadeh, *J. Taiwan Inst. Chem. Eng.* **2017**, *76*, 156; b) S. Khaisri, D. deMontigny, P. Tontiwachwuthikul, R. Jiraratananon, *J. Membr. Sci.* **2011**, *376*, 110; c) M. Simioni, S. E. Kentish, G. W. Stevens, *J. Membr. Sci.* **2011**, *378*, 18; d) R. Naim, A. Ismail, N. Cheer, M. Abdullah, *Chem. Eng. Res. Des.* **2014**, *92*, 1391; e) E. Kianfar, V. Pirouzfar, H. Sakhaeinia, *J. Taiwan Inst. Chem. Eng.* **2017**, *80*, 954; f) C. A. Scholes, S. E. Kentish, G. W. Stevens, D. deMontigny, *Int. J. Greenhouse Gas Control* **2016**, *55*, 195; g) H. J. Lee, M. K. Kim, J. H. Park, *Sep. Purif. Technol.* **2020**, *236*, 116304; h) Y. Guo, W. Qi, K. Fu, X. Chen, M. Qiu, Y. Fan, *Membranes* **2021**, *12*, 8.

[27] J. H. Lee, J. Kim, D. Liu, F. Guo, X. Shen, Q. Zheng, S. Jeon, J. K. Kim, *Adv. Funct. Mater.* **2019**, *29*, 1901623.

[28] J. A. Franco, S. E. Kentish, J. M. Perera, G. W. Stevens, *Ind. Eng. Chem. Res.* **2011**, *50*, 4011.